RSC Advances

PAPER

View Article Online
View Journal | View Issue

Cite this: *RSC Adv.*, 2022, **12**, 34165

Activated carbon prepared by co-pyrolysis of waste tobacco straw and waste LDPE mulch film: characterization and application for methylene blue removal†

Tianliang Zhang,[a] Wei Xiong,[b] Haiyan Zhang[b] and Jun Li*[a]

Efficient and inexpensive sorbents play a key role in removing organic pollutants from water bodies. In this study, a series of high surface area activated carbons (ACs) with excellent adsorption performance was prepared by co-pyrolysis of the waste tobacco straw and the waste low-density polyethylene (LDPE) mulch film. Using the maximum adsorption capacity of methylene blue (MB) as an indicator, the variables such as LDPE content, K_2CO_3 to raw material ratio, activation time, and activation temperature were optimized. The optimal synthesis conditions were as follows: LDPE content of 40%, K_2CO_3/raw material ratio of 1 : 2, activation temperature of 900 °C, and activation time of 100 min. The maximum adsorption capacity of MB was up to 849.91 mg g^{-1}. The results of scanning electron microscopy (SEM), X-ray powder diffraction (XRD), Raman, X-ray photoelectron spectroscopy (XPS), and BET showed that the moderate addition of LDPE was beneficial to the pyrolysis of the waste tobacco straw, bringing about the enrichment of surface groups (–OH, –COOH) and increasing its specific surface area and pore volume (up to 1566.7 m^2 g^{-1} and 0.996 cm^3 g^{-1}, respectively). The equilibrium data of MB adsorption by the composite activated carbon (PAC) was consistent with the Langmuir isotherm, while the adsorption kinetics were better described by a pseudo-second-order kinetic model. This work reveals the feasibility of LDPE mulch film and waste tobacco straw as potential and inexpensive precursors for preparing high surface area AC adsorbents.

Received 30th September 2022
Accepted 21st November 2022

DOI: 10.1039/d2ra06153h

rsc.li/rsc-advances

1 Introduction

Dyeing technology has emerged with the development of human society. Dyestuffs are widely used and applied in paints, cosmetics, textiles, and paper products. Releasing dyestuffs directly without treatment could cause serious pollution to the water environment. Methylene blue (MB) is a basic cationic dye widely used in printing and dyeing due to its strong dyeing ability. High-concentration of MB in water will not only affect the growth of aquatic organisms but also cause liver and digestive system damage in long-term drinkers, nausea, increased heart rate, epilepsy, and other symptoms.[1] To treat these printing and dyeing sewage in large quantities and at a low cost, researchers have tried various attempts, such as adsorption,[2] photocatalysis,[3] oxidation[4] and coagulation,[5] and membrane separation.[6] Compared with other methods, adsorption is simpler, cheaper, and more efficient, resulting in more application prospects.

Activated carbon generally has a high specific surface area, diverse surface groups, and developed pore structure, which endows it with strong adsorption capacity. Thus, activated carbon has been regarded as the most common adsorbent used to treat various water pollutants. However, the high regeneration cost of commercial activated carbon has prompted researchers to continue to look for cheaper alternatives. In the past decade, researchers have studied the production of activated carbon from rice husks,[7] bagasse,[8] bamboo,[9] garlic peel,[10] cotton stalk,[11] hazelnut shell,[12] peanut shell,[13] Fruit Stones and Nut Shells.[14] The advantage of using agricultural by-products for preparing activated carbon is that these raw materials are renewable and potentially less expensive.

China is the largest tobacco producer and consumer in the world,[15] and tobacco straw is the most significant by-product of tobacco production. Every year, a large amount of tobacco straw is discarded without reasonable utilization. These wastes contain a lot of nicotine and tar; direct incineration will produce a large amount of toxic and harmful gases, seriously polluting the environment. In addition, LDPE mulch films, the most widely used mulch films worldwide,[16] are widely used in tobacco growing processes. These mulch films are often mixed with waste tobacco straw and remain in the soil. If not handled properly, discarded mulch films will damage the soil structure,

[a]Sichuan University School of Chemical Engineering, Chengdu, 610000, China. E-mail: lijun@scu.edu.cn; scu_ztl@yeah.net

[b]Sichuan Tobacco Quality Supervision and Testing Station, Chengdu 610000, China

† Electronic supplementary information (ESI) available. See DOI: https://doi.org/10.1039/d2ra06153h

pollute the land, and reduce crop yields.[17] Solving the resource utilization of this mixed waste is a daunting task for researchers. In recent years, some studies on the preparation of AC from tobacco straw have been reported in the literature.[18–21] Tobacco straw was proved to be a potential raw material for preparing activated carbon. Activated carbons prepared from tobacco straw were efficient adsorbents for the removal of mercury,[22] Cr(VI),[23] Cr(III),[24] and methylene blue[21] from aqueous solutions. However, as far as we know, these studies only focus on tobacco straw, and there is no relevant research on preparing activated carbon adsorbents by mixing LDPE and tobacco straw.

In this study, a composite activated carbon (PAC) was prepared by co-pyrolysis using waste tobacco straw and waste LDPE mulch film. The effect of the addition of LDPE was investigated by characterization methods. In addition, the adsorption mechanism of MB on PAC was investigated by analyzing the adsorption behavior, adsorption isotherms, and adsorption kinetics. The aim was to provide a new efficient and economical adsorbent for organic dyes in wastewater.

2 Experimental

2.1 Materials

The waste tobacco straw and waste LDPE mulch film were provided by the Sichuan Provincial Tobacco Bureau Quality Supervision Station. It was cleaned, dried, pulverized, and then passed through a 100-mesh sieve. K_2CO_3 and HCl were purchased from Kelong Chemical Co., Ltd (Chengdu, China). MB was acquired from Jinsan Chemical Reagent Co., Ltd (Chengdu, China). The chemical structure of the dye is shown in Fig. 1. All other chemicals were used without further purification.

2.2 Single-step activation for the preparation of activated carbon

Tobacco straw powder, LDPE powder, and solid K_2CO_3 were added to the mortar in proportions, then ground thoroughly to make a homogeneous mixture. The mixed sample was placed in a boat-shaped crucible, heated to a predetermined temperature in a tube under the protection of an argon atmosphere, and thermostated for some time, then cooled to room temperature. Subsequently, the samples were transferred to beakers and stirred with dilute hydrochloric acid for several hours to remove the remaining activation agents and metal ions, and then washed with deionized water until the pH of the wash solution reached 6–7.

Activated carbon samples with different LDPE contents were labeled as PAC-x (x is the LDPE content, = 0, 0.2, 0.4, 0.6, 0.8). The LDPE content (ω) can be calculated by the following form:

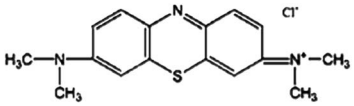

Fig. 1 Chemical structures of MB.

$$\omega = \frac{M_p}{M_c + M_p} \quad (1)$$

where M_p is the mass of LDPE; M_c is the mass of tobacco straw powder.

2.3. Characterization

The morphology and structure of the activated carbon were characterized by scanning electron microscopy (SEM, SU3500, Japan), equipped with EDX (energy dispersive X-ray) system to perform the elemental mapping and energy-dispersive spectrum (EDS) characterization. The crystalline structure of the samples was analyzed by the X-ray diffraction (XRD, Empyrean, Holland) in the 2θ range of 10–80° with a Cu-Kα X-ray source (λ = 1.54 Å). The graphitization degree was characterized by Raman spectrometer (LabRAM HR, French), and the Raman filter was 532 nm. The surface chemical composition was investigated by the X-ray photoelectron spectroscopy (XPS, AXIS Supra, UK) using monochromatic Al kα radiation. The specific surface area and pore size distribution was analyzed by an automatic specific surface area and porosity analyzer (ASAP 2460, USA) at 77 K. The concentration of methylene blue was determined by a double-beam UV spectrophotometer (MAPADA P5, China) at 665 nm.

2.4. MB adsorption experiments

The adsorption experiments were carried out in a 100 mL stoppered conical flask, which contained 20 mg of activated carbon and 50 mL of MB solution (500 mg L^{-1}). Then the mixture was placed in the thermostatic oscillator, oscillating at 150 rpm at 25 °C for 12 h to reach the adsorption equilibrium of the solid–solute mixture. The flask was removed from the thermostatic oscillator, and the final dye concentration in the solution was analyzed. The samples were filtered prior to analysis to minimize interference of the carbon fines with the analysis. The sampling and testing procedure were repeated three times, and the deviation of the data was expressed as an error bar.

The amount of adsorption at equilibrium, q_e (mg g^{-1}), was calculated by:

$$q_e = \frac{(C_0 - C_e)V}{m} \quad (2)$$

where m (g) and V (ml) are the mass of the activated carbon and the volume of MB solution, C_0 (mg L^{-1}) and C_e (mg L^{-1}) refer to the initial MB concentration, and the MB concentration at adsorption equilibrium, respectively.

2.5. MB adsorption kinetic studies

The procedures of kinetic experiments were basically identical to those of equilibrium tests. The stock solution of 1000 mg L^{-1} of MB was prepared using MB reagent and deionized water. Different concentrations of MB solutions were prepared by diluting these stock solutions. The adsorbate–adsorbent mixtures were collected at preset time intervals, and the concentration of the dye was measured after filtration. The

amount of adsorption at time t, q_t (mg g^{-1}) was calculated by the following formula:

$$q_t = \frac{(C_0 - C_t)V}{m} \quad (3)$$

where C_0 and C_t (mg L^{-1}) are the liquid-phase concentrations of MB at initial and any time t, respectively. V is the volume of the MB solution (l), and m is the mass of activated carbon (g).

3 Results and discussion

3.1 Optimization of preparation parameters

3.1.1 Effect of LDPE content on MB adsorption. The effect of LDPE content on MB adsorption is shown in Fig. 2(a). With the increased of LDPE content, the adsorption capacity of activated carbon for MB increased first and then decreased. The maximum amount of MB adsorption (804.22 mg g^{-1}) was reached when the LDPE content was 40%.

The difference in adsorption capacity may be related to the synergistic effect of LDPE in co-pyrolysis. Co-pyrolysis of biomass with polymers can improve the properties of biochar and increase its adsorption capacity.[25] According to the TGA measurement (Fig. S1), the decomposition temperature range of tobacco straw was between 180 °C and 510 °C, while the pyrolysis temperature of LDPE was 400–500 °C. The pyrolysis temperature of tobacco straw is lower than that of LDPE. When the mixture was fed into the tube furnace, the tobacco straw was decomposed first, and some free radicals, such as OH radical, were generated.[27] These active free radicals could react with the LDPE to accelerate the pyrolysis of LDPE.[26,28] The LDPE was an excellent hydrogen donor during co-pyrolysis reactions, which promoted the release of small-molecule volatile from tobacco straw by the radical interaction,[29,30] resulting in cavities on the surface and inside the activated carbon. These cavities could provide more adsorption sites for MB adsorption, so the adsorption capacity of activated carbon was improved. However, when the LDPE content was too high, the synergistic effect would lead to a high weight loss of activated carbon,[31] resulting in the collapse of the formed cavities and causing a decrease in adsorption capacity.

3.1.2 Effect of K_2CO_3 ratio on MB adsorption. Fig. 2(b) shows the effect of mass ratios of K_2CO_3 to mixed waste on MB adsorption. As shown in Fig. 2(b), MB adsorption capacity increased with increasing K_2CO_3 ratio from 1 : 1 to 2 : 1. It reached the maximum value when the ratio was 2 : 1. The adsorption capacity of MB decreased when the K_2CO_3 ratio was further increased to 2.5 : 1.

The change in adsorption capacity is related to the activation of K_2CO_3, and a similar trend has been reported by other researchers.[32,33] The process of mixed waste activation in a high temperature inert gas atmosphere may include the following redox reactions:[34]

$$K_2CO_3 \rightarrow K_2O + CO_2 \quad (4)$$

$$K_2CO_3 + 2C \rightarrow 2K + 3CO \quad (5)$$

$$K_2O + C \rightarrow 2K + CO \quad (6)$$

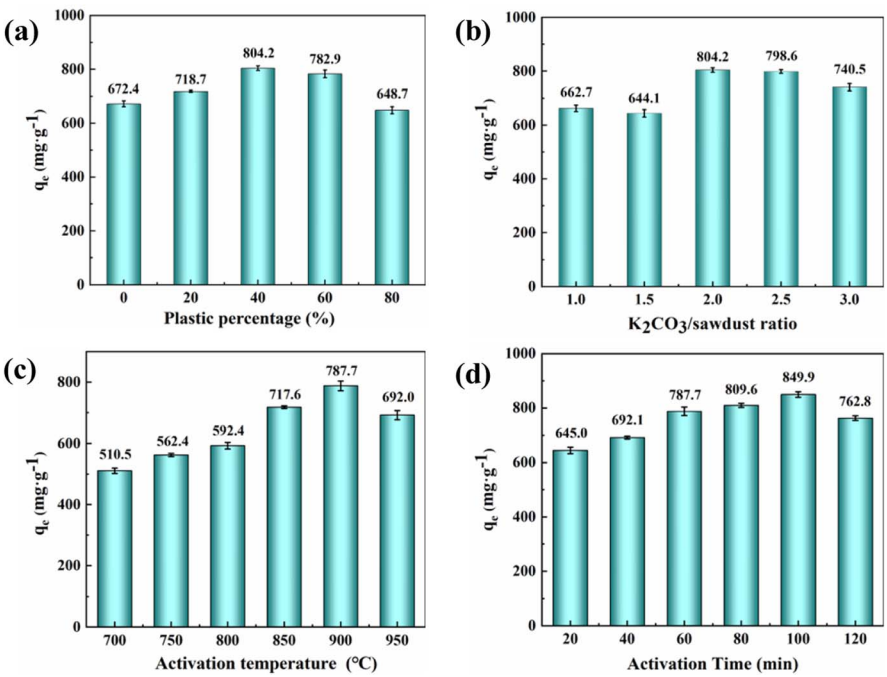

Fig. 2 Effects of preparation conditions on MB adsorption capacity. (a): The MB adsorption capacity of sample with LDPE content (%). (b): The MB adsorption capacity of sample with K_2CO_3/raw material ratio. (c): The MB adsorption capacity of sample with activation temperature. (d): The MB adsorption capacity of sample with activation time.

During the activation process, K_2CO_3 first decomposed into CO_2 and K_2O. Subsequently, the K_2O and the rest of K_2CO_3 reacted with the carbon atoms in the mixed waste to form potassium atoms and carbon monoxide.[35] The porous structure was formed on the surface of the activated carbon by the collaborative results of chemical activation, physical activation (CO_2),[36] and the expansion of the carbon lattices by metallic potassium.[37,38] The K_2CO_3 activation promoted the generation of pores on activated carbon, which brought about an increase of the adsorption capacity. It is worth noting that if the K_2CO_3 ratio was too high, more potassium atoms would enter the carbon lattice, causing the collapse of the pore structure.[35] It would result in a reduction in the adsorption capacity of the activated carbon.

3.1.3 Effect of activation temperature on MB adsorption. The activated carbon adsorption capacity for MB with different activation temperatures is shown in Fig. 2(c). It can be clearly seen that the adsorption value of MB on activated carbon with the activation temperature increased first and then decreased. The adsorption amount at 900 °C reached the maximum value: 804.22 mg g^{-1}.

Temperature is also important in preparing activated carbon and can affect its adsorption capacity. Since K_2CO_3 activation requires a certain temperature, increasing the activation temperature facilitates the activation process. When the activation temperature exceeded the boiling point of metallic potassium (762 °C), a large amount of potassium vapor was generated and entered the internal pores, promoting the opening of the carbon lattice and increasing the pore volume of the activated carbon.[39] On the other hand, as the temperature increased, the cross-linked structures in activated carbon would also gradually decompose.[40] It would release the blocked pores, causing an increase in specific surface area and pore volume. This may be why the adsorption capacity of activated carbon on MB increases gradually with temperature in the early stage. As the temperature continued to increase (950 °C), the pore size continued to expand, leading to the collapse of the pore structure and a decrease in adsorption capacity.

3.1.4 Effect of activation time on MB adsorption. Fig. 2(d) shows the relationship between the MB adsorption capacity of activated carbon and different activation times (t). The adsorption of MB by activated carbon increased and then decreased with increasing activation time, with a peak at 100 min: 849.91 mg g^{-1}.

The reason may be that the K_2CO_3 needs enough time to pyrolyze into K_2O and CO_2 and give full play to the activation effect.[41] Extending the activation time is helpful for to the reaction of K_2CO_3 with C atoms, making the carbon material produce a large number of pore structures.[42] Therefore, when the activation time was extended from 20 min to 100 min, the adsorption capacity of activated carbon for MB was significantly improved. Continuing to extend the activation time (120 min), the K_2CO_3 would react with the carbon layer inside the pore, and the adjacent pore wall was destroyed, causing the collapse of the activated carbon pore and the decrease of adsorption capacity.[42]

3.2 Material characterization for PAC

Based on the above discussion, it was clear that the adsorption capacity of the prepared activated carbons was affected by the LDPE content, K_2CO_3/raw material ratio, activation temperature, and activation time. In order to study the effect of LDPE content on activated carbon, other factors were controlled as optimal conditions: K_2CO_3/raw material ratio of 2 : 1, activation temperature of 900 °C, and activation time of 100 min.

3.2.1 Morphological characterization. The surface topography of the prepared PAC was investigated by SEM. The images of PACs show that the PACs are loose, and a large number of pores are developed on the surface (Fig. 3(a)–(c)). Depending on the LDPE content, the external surface of the SACs has pores with different numbers and sizes. It can be seen that the surface of PAC-0 without LDPE addition is flatter with a smaller size of pores. In contrast, the samples PAC-0.4 and PAC-0.8 with LDPE addition have more large round pores (Fig. 3(d)–(f)). The comparison of surface morphology verifies the facilitation of biomass pyrolysis by LDPE, which generates volatile substances resulting in pore size expansion.[43] EDS spectrum and elemental mapping images of PAC-0.4 (Fig. 3(g)–(i)) reveal that PACs are primarily composed of C, with a small amount of O.

3.2.2 Structural characterization (XPS/XRD/Raman). Fig. 4(a) shows the powder X-ray diffraction (XRD) patterns of PAC-0, PAC-0.4, and PAC-0.8. All PAC-x show similar diffraction peak structures at 22° and 44°, corresponding to the (002) and (100) crystallographic planes of the crystals, respectively.[44] It implies that these samples have a typical amorphous carbon structure and contain a certain amount of graphite microcrystals.[45]

Raman can show the difference in the graphitization degree of the samples more clearly. As shown in Fig. 4(b), there are two drum peaks and one obtuse peak located at 1350 cm^{-1}, 1585 cm^{-1}, and 2760 cm^{-1}, corresponding to the D peak (disorder peak), G peak (graphite peak) and 2D peak, respectively. The 2D peak is used to characterize the sample's stacking pattern of C atoms.[46] The ratio of D and G peak intensities (I_D/I_G) can be used to evaluate the degree of graphitization and defects in carbon material,[47] with larger values of I_D/I_G representing a higher degree of material defects. With the addition of LDPE, the I_D/I_G ratio of the samples increased from 0.95 to 1.00–1.01. The increasing trend is also accompanied by an increase in the peak intensity of the 2D band. It indicates that the addition of LDPE would promote the pyrolysis process, resulting in the destruction of the ordered initially graphitized structure, thus, the formation of more defects, which would provide more active sites and improve its adsorption performance.

To further reveal the elemental binding on the activated carbon surface, the XPS was used. The overall peak in C 1s XPS spectrum of PAC-0.4 can be deconvoluted to four individual C peaks components: C=C (248.7 eV), C–O (285.6 eV), C=O (286.9 eV), and O–C=O (289.3 eV) (Fig. 5(a)). Likewise, the overall peak in O 1s XPS spectrum of PAC-0.4 can also be deconvoluted to three individual O peaks components: C=O (532.5 eV), C–OH (533.2 eV), and COOH (533.8 eV) (Fig. 5(b)). Studies have shown that when activated carbon was placed in

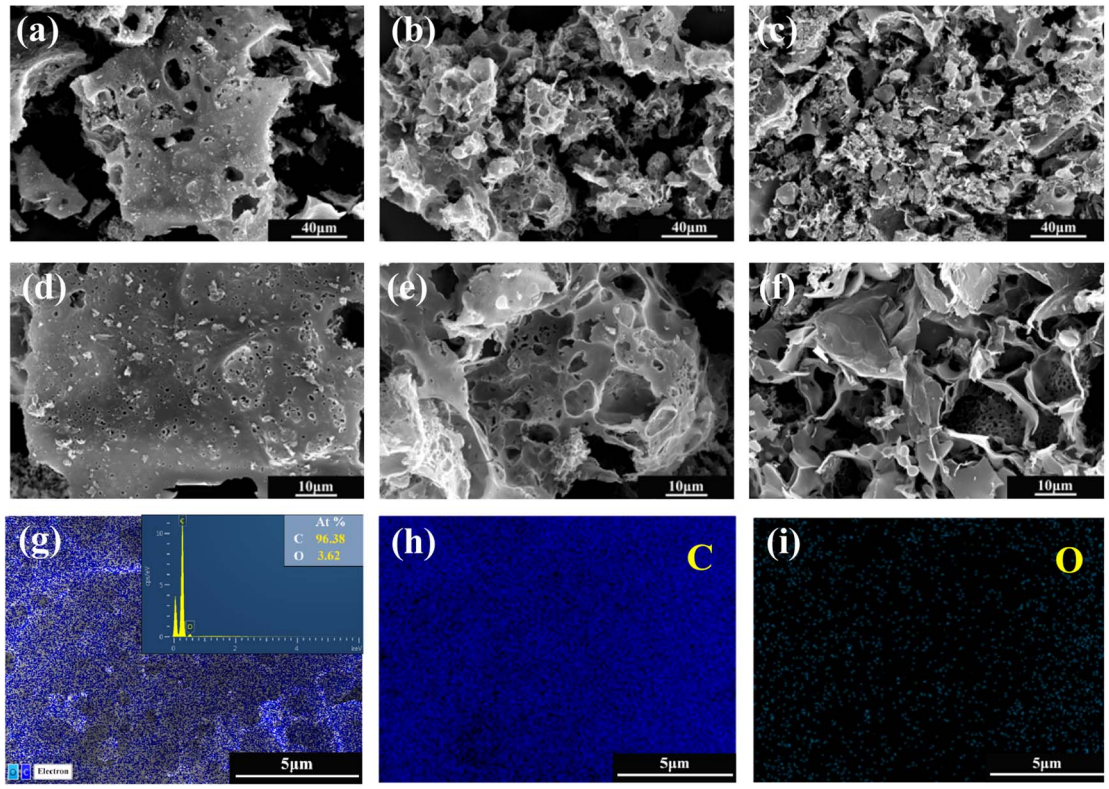

Fig. 3 The SEM images of PAC-0 (a and d), PAC-0.4 (b and e), PAC-0.8 (c and f), EDS spectrum and elemental mapping images of PAC-0.4 (g–i).

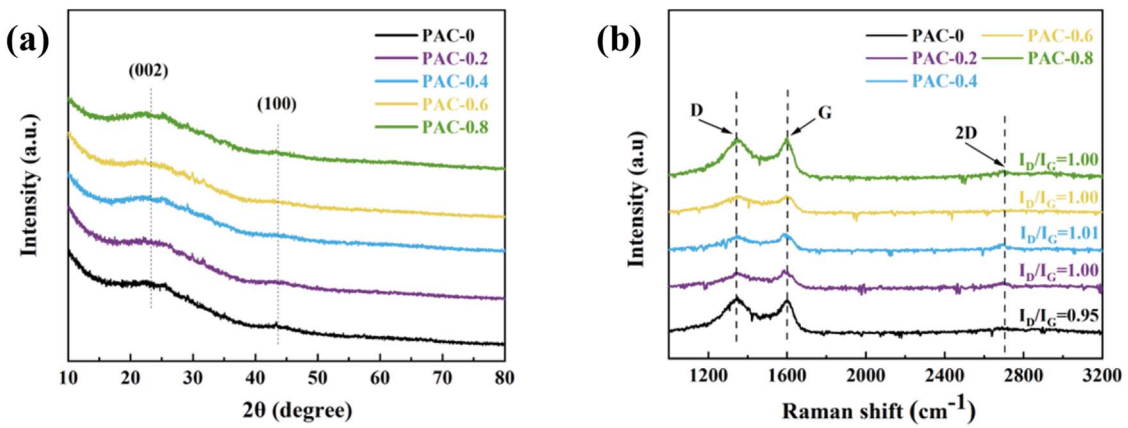

Fig. 4 XRD patterns (a) and Raman spectra (b) of samples with different LDPE contents.

an aqueous solution, the acidic surface groups on the carbon surface were susceptible to ionization, producing H ions directed toward the liquid phase, leaving the carbon surface with negatively charged sites.[48,49]

$$>C–OH \rightleftharpoons >C{=}O + H^+ + e^- \quad (7)$$

$$–COOH \rightleftharpoons –COO + H^+ + e^- \quad (8)$$

$$>C{=}O + e^+ \rightleftharpoons >C–O^- \quad (9)$$

This makes it easier for the activated carbon to adsorb cationic molecules by electrostatic interaction and also reasonably explains the extremely high adsorption capacity of PAC on cationic MB.

3.2.3 Pore structure characterization (BET). According to IUPAC, the physical adsorption isotherms can be divided into six major categories, and the various adsorption isotherms in practice are different combinations of these six major categories.[50]

Fig. 6(a) shows the nitrogen (N_2) adsorption isotherms of three samples prepared with different LDPE contents, and all

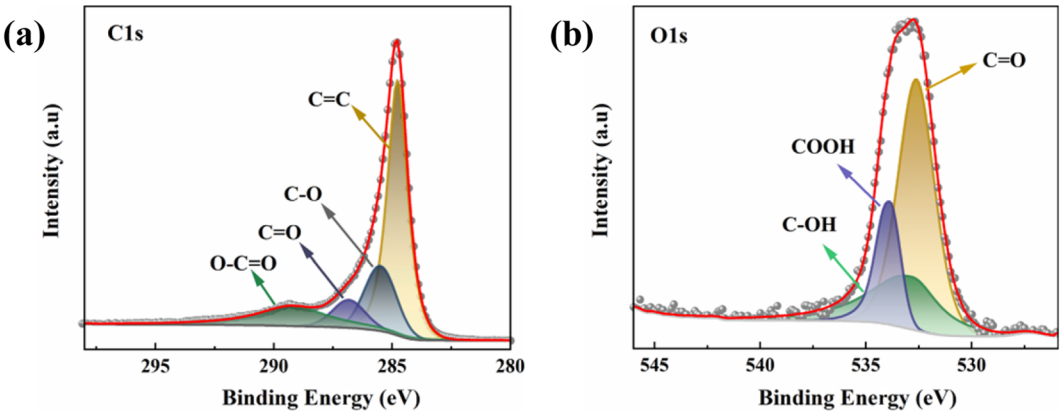

Fig. 5 XPS spectrum of PAC-0.4: C 1s spectrum (a); O 1s spectrum (b).

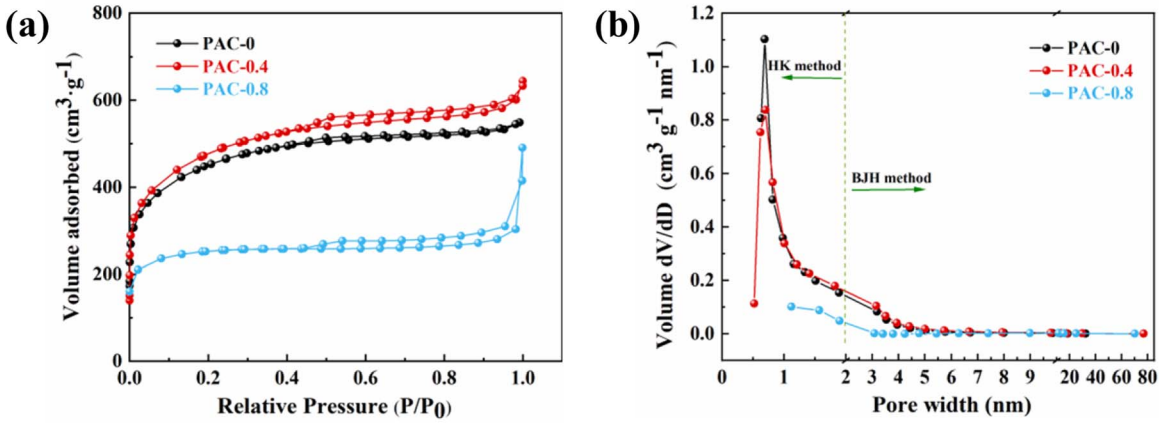

Fig. 6 (a) Nitrogen adsorption–desorption isotherms; (b) pore size distribution for PAC-0, PAC-0.4, and PAC-0.8.

curves exhibit a mixed I/IV pattern. Under the condition of very low relative pressures ($P/P_0 < 0.01$), the N_2 adsorption of the material increased rapidly with increasing relative pressure. When the relative pressure increased to ($0.1 < P/P_0 < 0.5$), the growth rate of N_2 adsorption of the material gradually slowed down, and a plateau appeared in the adsorption curve. That coincides with the type I adsorption curve and proves that the material has a typical microporous structure; when the relative pressure continued to increase to ($0.5 < P/P_0 < 0.9$), H4 hysteresis loops appeared in all isothermal curves, which coincided with the IV adsorption curves, indicating the presence of a large number of mesoporous structures. The hysteresis loops of PAC-0.4 and PAC-0.8 were more obvious than those of PAC-0, indicating that the number of mesopores may be more abundant. The pore size distributions of them are shown in Fig. 6(b), the micropores and mesopores are all distributed, and the mesopores are mainly distributed at 3–8 nm. Table 1 lists the specific surface areas (SSAs) and other porous structure parameters for PAC-0, PAC-0.4, and PAC-0.8. PAC-0.4 has the largest specific surface area among the three samples, and LDPE obviously has an important effect on promoting the formation of porous structures. It can be seen that with the increase of LDPE content, the pore capacity of PAC-0.4 compared with PAC-0 micropores and mesopores both increased, indicating that LDPE can not only induce the activated carbon to produce new pores but also induce the micropores further to expand and form mesopores. The high V_{meso} and the sharply reduced V_{micro} exhibited by PAC-0.8 proves that too much LDPE will cause excessive pyrolysis, and some pore walls will collapse, as evidenced by the SEM image of PAC (Fig. 2).

Table 1 Pore structure data of samples with different LDPE contents

Samples	S_{BET} ($m^2\ g^{-1}$)	V_{total} ($cm^3\ g^{-1}$)	V_{meso} ($cm^3\ g^{-1}$)	V_{micro} ($cm^3\ g^{-1}$)	V_{meso}/V_{total} (%)
PAC-0	1454.4954	0.847902	0.180635	0.693148	21.30
PAC-0.4	1566.7029	0.996131	0.306523	0.731457	30.77
PAC-0.8	773.1014	0.758242	0.372582	0.389571	49.14

3.3. Adsorption kinetic study

The adsorption kinetics describes the adsorption rate of the adsorbent to the target pollutant, which is of great significance for exploring the adsorption mechanism. Pseudo-first-order (PFO)[51] and pseudo-second-order (PSO)[52] kinetic models were used to fit the experimental data to understand the MB adsorption process by evaluating the kinetic adsorption parameters. The model equation is as follows:

$$\ln(q_e - q_t) = \ln(q_e) - k_1 t \quad (10)$$

$$\frac{t}{q_t} = \frac{1}{k_2 q_e^2} + \frac{1}{q_e} t \quad (11)$$

where k_1 (min^{-1}) and k_2 (g mg^{-1} min^{-1}) are the absorption rate constants of pseudo-first-order and pseudo-second-order models. q_t and q_e (mg g^{-1}) are the MB adsorption capacity at a certain time and the equilibrium adsorption capacity, respectively.

From Fig. 7 and Table 2, it can be concluded that the proposed second-order model has a higher correlation coefficient (R^2 > 0.999), a better fit, and the predicted adsorption values deviate less from the experimental values. Therefore, the adsorption process of MB on PAC-0.4 followed the proposed second-order kinetic model, which was dominated by chemisorption. The results obtained in this study are consistent with the previously reported studies on the adsorption of MB on other ACs.

The adsorption of MB on PAC may include several steps such as external diffusion and intraparticle diffusion. The pseudo-first- and second-order kinetic models could not determine the diffusion mechanism. In order to further investigate the adsorption process, an intraparticle diffusion model was used to fit the process of MB adsorption by PAC. The intraparticle diffusion model equation is expressed as:

$$q_t = k_i t^{0.5} + c \quad (12)$$

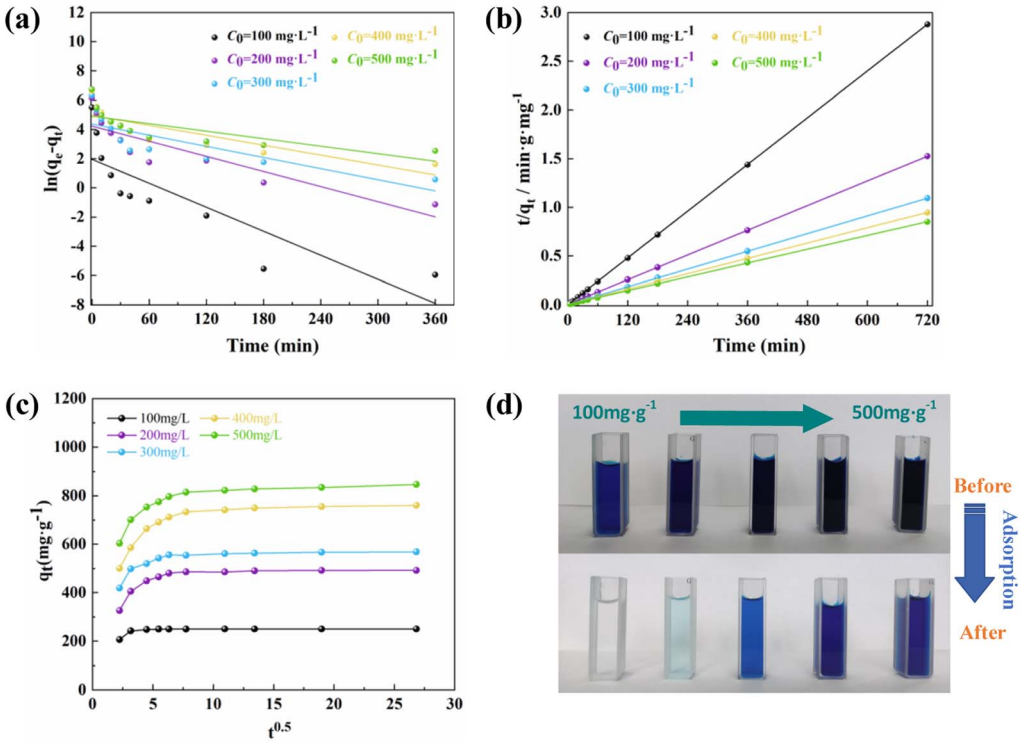

Fig. 7 Fitted adsorption kinetics of MB on PAC-0.4. (Pseudo-first-order kinetic (a), pseudo-second-order kinetic (b)); intraparticle diffusion model curve for MB adsorption on PAC-0.4 (c); comparison of MB solutions before and after adsorption (d).

Table 2 Parameters of pseudo-first-order and pseudo-second-order kinetic models for MB removal on PAC-0.4

C_0 (mg L^{-1})	Pseudo-first-order			Pseudo-second-order		Experimental values	
	q_{e1} (mg g^{-1})	k_1 (min^{-1})	R^2	q_{e2} (mg g^{-1})	k_2 (g mg^{-1} min^{-1})	R^2	q_e (mg g^{-1})
100	7.0995	0.0274	0.7204	250.0001	0.0143	1	249.9951
200	69.1232	0.0173	0.7810	473.9336	0.0012	0.9999	471.8685
300	79.5861	0.0127	0.6559	657.8947	0.0011	1	658.4287
400	143.3000	0.0113	0.7056	763.3588	0.0004	0.9999	760.4105
500	136.2389	0.0086	0.5677	847.4576	0.0004	0.9999	846.7742

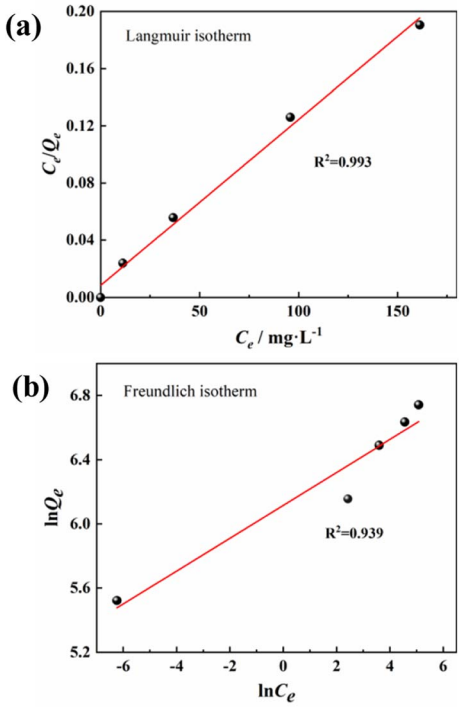

Fig. 8 Adsorption isotherm of Langmuir (a), Freundlich (b).

where k_i is the intraparticle diffusion rate constant, and c (mg g^{-1}) is the intercept reflecting the boundary layer effect. Parameters (k_i, c) can be calculated from the intercept and slope of the linear plots. Fig. 7(c) shows that the slope increased and the intercept decreased as the initial MB concentration increased from 100 mg L^{-1} to 500 mg L^{-1}. This phenomenon may be attributed to the increase in the boundary layer thickness and driving force resulting from the initial dye concentration. The curves at high concentration (200–500 mg L^{-1}) indicate that the adsorption process involves three stages: in the first stage, the initial stage of adsorption, the slope of the straight line is high, indicating that the adsorption was mainly controlled by the external diffusion process. In the second stage, as the adsorption proceeded, the adsorption sites of PAC-0.4 decreased, and the slope of the curve decreased, indicating that the adsorption was controlled by the intraparticle diffusion process. In the third stage, after the adsorption proceeded for 20 min, the adsorption sites were basically saturated, and the adsorption reached equilibrium. At low concentrations (100 mg L^{-1}), the adsorption of MB on PAC-0.4 reached equilibrium quickly and was mainly controlled by the external diffusion process.

Fig. 8(d) shows that MB could be completely removed by PAC-0.4 at low concentrations, so we predict that PAC-0.4 can be applied to real MB contamination adsorption in the future.

3.4. Isotherm study

Adsorption isotherms are often used to describe adsorbates–adsorbents interactions and the equilibrium distribution of adsorbate molecules in the solid–liquid phase.[53] The experimental data were further analyzed using Langmuir[54](13) and Freundlich[55] (15) isotherm models to evaluate the interaction and maximum adsorption of MB dyes by activated carbon.

$$\frac{C_e}{q_e} = \frac{1}{Q_0 b} + \left(\frac{1}{Q_0}\right) C_e \quad (13)$$

$$R_L = \frac{1}{1 + bC_0} \quad (14)$$

$$\ln q_e = \ln K_F + \left(\frac{1}{n}\right) \ln C_e \quad (15)$$

where C_e is the equilibrium concentration of MB, q_e is adsorption capacity at equilibrium adsorption. Q_0 and b are Langmuir constants related to adsorption capacity and rate of adsorption, respectively. C_0 is the initial concentration of MB. K_F and n are Freundlich constants, n giving an indication of how favorable the adsorption process and K_F is the adsorption capacity of the adsorbent.

The Langmuir adsorption model assumes that the adsorption capacity of a solid adsorbent is limited. The same active sites are evenly distributed over the adsorbent surface, and each activation site is bound to only one adsorbate molecule. In contrast, the Freundlich adsorption model considers the existence of different types of active sites with different adsorption capacities on the adsorbent surface, describing a multilayer adsorption process on adsorbent molecules. As can be seen from the parameters in Fig. 8 and Table 3, the PAC adsorption process matches the Langmuir model better (R^2 = 0.993), and the process is single molecular layer adsorption. The maximum adsorption amount was 862.07 mg g^{-1}, which is very similar to the actual experimental (849.91 mg g^{-1}) and kinetically fitted values (847.45 mg g^{-1}).

In addition, the separation factor R_L is an important Langmuir isotherm parameter that can be used to predict the interaction of the adsorbent with the adsorbate in an aqueous solution. The magnitude of the R_L value reflects the type of adsorption process: unfavorable (R_L > 1); Linear (R_L = 1); favorable (0 < R_L < 1); irreversible (R_L = 0). The R_L for PAC adsorption of MB is 0.0143–0.0678, indicating that the adsorption process occurred readily and was irreversible.

Table 4 compares the surface area and adsorption capacity of several bio-sorbents with PAC for MB dyes. The PAC-0.4 possesses a higher specific surface area and a stronger adsorption capacity for MB dye compared to other ACs prepared from lignocellulosic biomass. Therefore, the activated carbon

Table 3 Isotherm parameters for MB adsorption on PAC

Model	Parameter	
Langmuir	b	0.137
	Q_0	862.069
	R^2	0.993
	R_L	0.0143∼0.0678
Freundlich	K_F	452.691
	n	9.75
	R^2	0.94

Table 4 Comparison of adsorption capacity of PAC-0.4 with others AC for MB

Raw materials	S_{BET} ($m^2\ g^{-1}$)	Adsorption capacity ($mg\ g^{-1}$)	References
Tobacco straw and LDPE mulch film	**1566.70**	**849.91**	**This work**
Globe artichoke	2038	780	56
Sucrose	1534	704.2	57
Rice husks	2028	578	58
Potato residue	1357	540	58
Hazelnut shells	1335	524	59
Oil palm	707.79	312.5	60
Bamboo	1323	286.1	9
Karanj fruit hulls	849.66	239.4	61
Mangosteen peel	1622	1192	62

prepared from waste tobacco straw and waste LDPE mulch film in this study is an efficient adsorption material for removing hardly degradable organics contaminants in water.

3.5. MB adsorption mechanism

FTIR analysis of PAC-0.4 before and after MB adsorption was performed to explore its adsorption mechanism for MB. Fig. 9 shows the FTIR spectra recorded for the samples in the range from 500 to 4000 cm^{-1}. The broad absorption peak around 3425 cm^{-1} is attributed to the O–H stretching vibration. The band at 2921 cm^{-1} and its shoulder at 2849 cm^{-1} are attributed to νC–H and δC–H (ν = stretching and δ = bending) absorption bands, respectively, which indicates the presence of methyl and methylene groups in the precursor.[63] The peak around 2302 cm^{-1} corresponds to the stretching vibration peak of the O–H bond in the COOH functional group,[64] while the characteristic peak at 1632 cm^{-1} is ascribed to the –C=C– stretching vibration. After MB adsorption, the peak around 3425 cm^{-1} caused by O–H stretching vibration became narrower and the peak intensity was decreased, while the C=C peak at 1632 cm^{-1} was shifted to 1592 cm^{-1}. In addition, many small peaks occurred between 1050 cm^{-1} and 1400 cm^{-1}, which is attributed to the MB, indicating that the MB dye cation was adsorbed to the surface of PAC. No new characteristic peaks appear before and after adsorption, indicating that the adsorption of MB by PAC-0.4 is physical adsorption.

Furthermore, many researchers report that the adsorption process of MB is significantly influenced by the solution pH.[65–67] Therefore, we investigated the relationship between the adsorption of MB by PAC and the pH of the solution. The maximum MB adsorption capacity of PAC-0.4 under different solution pH is shown in Fig. 10(a). It can be seen that increasing the solution pH contributes to improving the adsorption capacity, with a significant increase in adsorption capacity as the pH increases from 6 to 8. This may be related to the pH_{pzc} of PAC, defined as the pH at which the net surface charge is zero. Fig. 10(b) shows that the pH_{pzc} of PAC-0.4 is 6.26. When the solution pH < pH_{pzc}, the adsorbent reacts as a positive surface, and as a negative surface when the solution pH > pH_{pzc}.[68] The inhibition of MB adsorption under low pH conditions can be attributed to the electrostatic repulsion between the positively charged adsorbent surface and the cationic MB molecules, and the presence of excess H ions competing with dye cations for the adsorption sites. As the pH increases, the number of hydroxyl groups on the surface of activated carbon increases, thus increasing the number of minus charge sites.[69] With the negative charge neutralizes the positive charge on the surface, a negative charge is eventually generated on the adsorbent surface. The increased electrostatic attraction between PAC and MB facilitates the adsorption of MB by PAC.

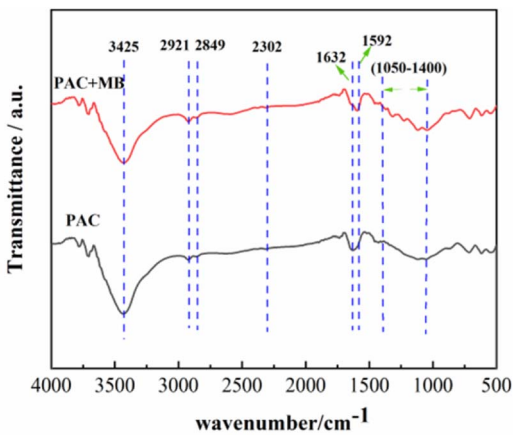

Fig. 9 FTIR spectra of before and after adsorption.

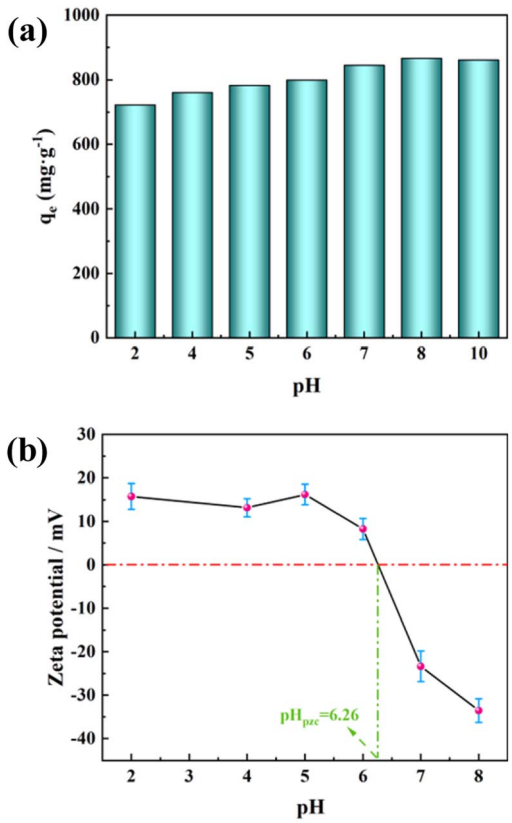

Fig. 10 Effect of PH on MB adsorption capacity (a). The zeta potential of PAC-0.4 (b).

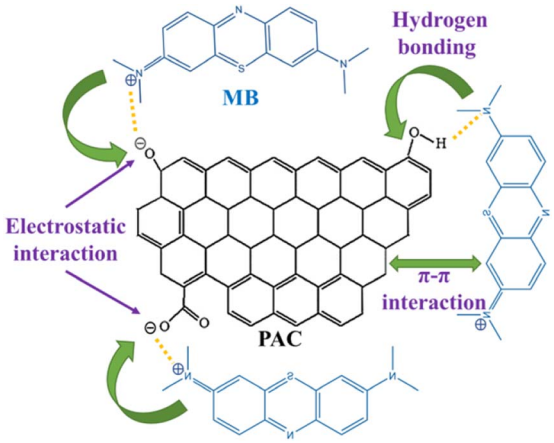

Fig. 11 Possible MB adsorption mechanism.

According to FTIR spectra, combined with BET, SEM characterization and adsorption experiments, the adsorption mechanism of PAC for MB is analyzed: (i) after adsorption, the peak of 3425 cm^{-1} caused by O–H stretching vibration is significantly reduced, indicating that oxygen-containing groups on the surface of PAC, such as – COH, can adsorb some MB molecules through hydrogen bonding. (ii) Adsorption of MB on PAC is favored by the alkaline conditions, indicating that the positively charged MB molecules are easily adsorbed to the negatively charged PAC surface by electrostatic interaction. (iii) MB is an ideal planar molecule, and the aromatic backbone of MB dye can easily interact with PAC through π–π stacking,[70] contributing to the adsorption of MB onto the PAC surface. The possible MB adsorption mechanism onto PAC is schematically illustrated in Fig. 11.

4. Conclusions

In this study, a series of activated carbon adsorbents (PAC) with a high specific surface area were prepared by co-pyrolysis of waste LDPE mulch film with waste tobacco straw. The addition of LDPE promotes the pyrolysis of tobacco straw, which brings higher specific surface area and larger pore volume. The sample prepared under optimal conditions has a maximum surface area of 1566.7 $m^2\ g^{-1}$ and is distributed with active groups favorable for MB adsorption. The maximum adsorption of MB is 849.91 mg g^{-1}, and the adsorption follows the adsorption pseudo-second-order kinetic model and Langmuir adsorption model. Compared with other reported biomass-activated carbon, PAC has higher adsorption efficiency and is an effective and economical material for removing dye contaminants from water. Based on the results of this work, waste LDPE mulch film and waste tobacco straw can be used as potential precursors for preparing AC with good surface properties and effective adsorption for numerous environmental applications.

Conflicts of interest

There are no conflicts to declare.

Acknowledgements

This work is supported by China National Tobacco Corporation Sichuan Province Science and Technology Program Project (SCYC201918).

References

1 A. Hassan, A. Abdel-Mohsen and M. M. Fouda, *Carbohydr. Polym.*, 2014, **102**, 192–198.
2 A. B. Albadarin, M. N. Collins, M. Naushad, S. Shirazian, G. Walker and C. Mangwandi, *Chem. Eng. J.*, 2017, **307**, 264–272.
3 M. Nawi, S. Sabar, A. Jawad and W. W. Ngah, *Biochem. Eng. J.*, 2010, **49**, 317–325.
4 Z. Eskandari, A. Talaiekhozani, M. R. Talaie and F. Banisharif, *J. Environ. Manage.*, 2019, **231**, 297–302.
5 N. d. C. L. Beluci, G. A. P. Mateus, C. S. Miyashiro, N. C. Homem, R. G. Gomes, M. R. Fagundes-Klen, R. Bergamasco and A. M. S. Vieira, *Sci. Total Environ.*, 2019, **664**, 222–229.
6 S. S. Shenvi, A. M. Isloor, A. F. Ismail, S. J. Shilton and A. Al Ahmed, *Ind. Eng. Chem. Res.*, 2015, **54**, 4965–4975.
7 N. Yalçin and V. Sevinç, *Carbon*, 2000, **38**, 1943–1945.
8 W. Tsai, C. Chang, M. Lin, S. Chien, H. Sun and M. Hsieh, *Chemosphere*, 2001, **45**, 51–58.
9 Q.-S. Liu, T. Zheng, N. Li, P. Wang and G. Abulikemu, *Appl. Surf. Sci.*, 2010, **256**, 3309–3315.
10 B. Hameed and A. Ahmad, *J. Hazard. Mater.*, 2009, **164**, 870–875.
11 H. Deng, L. Yang, G. Tao and J. Dai, *J. Hazard. Mater.*, 2009, **166**, 1514–1521.
12 M. Doğan, H. Abak and M. Alkan, *J. Hazard. Mater.*, 2009, **164**, 172–181.
13 M. A. Ahmad, M. F. M. Yusop, R. Zakaria, J. Karim, N. K. E. Yahaya, M. A. M. Yusoff, N. H. F. Hashim and N. S. Abdullah, *Mater. Today: Proc.*, 2021, **47**, 1246–1251.
14 A. Aygün, S. Yenisoy-Karakaş and I. Duman, *Microporous Mesoporous Mater.*, 2003, **66**, 189–195.
15 J. Mackay, *Br. Med. Bull.*, 2016, **120**, 15–25.
16 P. Tribedi and S. Dey, *Environ. Monit. Assess.*, 2017, **189**, 1–8.
17 R. Qi, D. L. Jones, Z. Li, Q. Liu and C. Yan, *Sci. Total Environ.*, 2020, **703**, 134722.
18 Z. Ma, B. Jiang, Q. Yuan, L. Cao, L. Liu, J. Tian, Z. Huang, Z. Zong, Z. Lin and P. Zhang, *Vib. proced.*, 2021, **39**, 121–127.
19 H. Yi, H. Deng, L. Yang, X. L. Tang, Q. Yu and Z. Ye, *Sep. Sci. Technol.*, 2013, **48**, 813–819.
20 J. Wang, B. Jiang, L. Liu, L. Cao, Q. Yuan, Z. Zong, Z. Huang, J. Tian, P. Zhang, Z. Lin and Z. Ma, *J. Phys.: Conf. Ser.*, 2022, **2160**, 012041.
21 B. Mudyawabikwa, H. H. Mungondori, L. Tichagwa and D. M. Katwire, *Water Sci. Technol.*, 2017, **75**, 2390–2402.
22 H. Zhang, T. Wang, Z. Sui, Y. Zhang, B. Sun and W.-P. Pan, *Fuel*, 2019, **253**, 703–712.
23 W. Tang, R. Zeng, Y. Feng, M. Liu, F. Zhang and G. Peng, *Chin. J. Environ. Eng.*, 2015, **9**, 5161–5166.
24 J. Pan, J. Jiang and R. Xu, *J. Environ. Sci.*, 2013, **25**, 1957–1965.

25 S.-Y. Oh and Y.-D. Seo, *Bioresour. Technol.*, 2016, **218**, 77–83.
26 L. Zhou, Y. Wang, Q. Huang and J. Cai, *Fuel Process. Technol.*, 2006, **87**, 963–969.
27 J. Yang, J. Rizkiana, W. B. Widayatno, S. Karnjanakom, M. Kaewpanha, X. Hao, A. Abudula and G. Guan, *Energy Convers. Manage.*, 2016, **120**, 422–429.
28 L. Zhou, T. Luo and Q. Huang, *Energy Convers. Manage.*, 2009, **50**, 705–710.
29 B. Han, Y. Chen, Y. Wu, D. Hua, Z. Chen, W. Feng, M. Yang and Q. Xie, *J. Therm. Anal. Calorim.*, 2014, **115**, 227–235.
30 V. S. Kaushik, C. S. Dhanalakshmi, P. Madhu and P. Tamilselvam, *Environ. Sci. Pollut. Res.*, 2022, 1–11.
31 A. Dewangan, D. Pradhan and R. Singh, *Fuel*, 2016, **185**, 508–516.
32 K. Foo and B. Hameed, *Bioresour. Technol.*, 2012, **111**, 425–432.
33 K. Foo and B. Hameed, *Chem. Eng. J.*, 2012, **180**, 66–74.
34 P. Ehrburger, A. Addoun, F. Addoun and J.-B. Donnet, *Fuel*, 1986, **65**, 1447–1449.
35 L. Li, C. Jia, X. Zhu and S. Zhang, *J. Cleaner Prod.*, 2020, **256**, 120326.
36 T. Yang and A. C. Lua, *J. Colloid Interface Sci.*, 2003, **267**, 408–417.
37 L. Yue, Q. Xia, L. Wang, L. Wang, H. DaCosta, J. Yang and X. Hu, *J. Colloid Interface Sci.*, 2018, **511**, 259–267.
38 J. Romanos, M. Beckner, T. Rash, L. Firlej, B. Kuchta, P. Yu, G. Suppes, C. Wexler and P. Pfeifer, *Nanotechnology*, 2011, **23**, 015401.
39 L. Li, Y. Lv, J. Wang, C. Jia, Z. Zhan, Z. Dong, L. Liu and X. Zhu, *Bioresour. Technol.*, 2022, **343**, 126101.
40 J. i. Hayashi, T. Horikawa, K. Muroyama and V. G. Gomes, *Microporous Mesoporous Mater.*, 2002, **55**, 63–68.
41 W. Jinzhou, M. Peiyong, Z. Xianwen, X. Xianjun and G. Xiaowei, *Acta Energ. Sol. Sin.*, 2019, **40**, 2113–2120.
42 I. I. Gurten, M. Ozmak, E. Yagmur and Z. Aktas, *Biomass Bioenergy*, 2012, **37**, 73–81.
43 Y. Zheng, L. Tao, X. Yang, Y. Huang, C. Liu and Z. Zheng, *J. Anal. Appl. Pyrolysis*, 2018, **133**, 185–197.
44 Y. Teng, E. Liu, R. Ding, K. Liu, R. Liu, L. Wang, Z. Yang and H. Jiang, *Electrochim. Acta*, 2016, **194**, 394–404.
45 Y. Gao, L. Li, Y. Jin, Y. Wang, C. Yuan, Y. Wei, G. Chen, J. Ge and H. Lu, *Appl. Energy*, 2015, **153**, 41–47.
46 L. Yang, S. Luo, F. Su, Y. Xiao, Y. Chen and Q. Cai, *J. Phys. Chem. C*, 2010, **114**, 7694–7699.
47 Y. Guo, Z.-q. Shi, M.-m. Chen and C.-y. Wang, *J. Power Sources*, 2014, **252**, 235–243.
48 B. S. Girgis, A. A. Attia and N. A. Fathy, *Colloids Surf., A*, 2007, **299**, 79–87.
49 E. Frackowiak and F. Beguin, *Carbon*, 2001, **39**, 937–950.
50 S. J. Gregg, K. S. W. Sing and H. Salzberg, *J. Electrochem. Soc.*, 1967, **114**, 279Ca.
51 S. Lagergren, *K. Sven. Vetenskapsakad. Handl.*, 1898, **24**, 1–39.
52 Y.-S. Ho and G. McKay, *Chem. Eng. J.*, 1998, **70**, 115–124.
53 V. Njoku, K. Foo, M. Asif and B. Hameed, *Chem. Eng. J.*, 2014, **250**, 198–204.
54 I. Langmuir, *J. Am. Chem. Soc.*, 1916, **38**, 2221–2295.
55 H. Freundlich, *J. Phys. Chem.*, 1906, **57**, 1100–1107.
56 M. Benadjemia, L. Millière, L. Reinert, N. Benderdouche and L. Duclaux, *Fuel Process. Technol.*, 2011, **92**, 1203–1212.
57 K. C. Bedin, A. C. Martins, A. L. Cazetta, O. Pezoti and V. C. Almeida, *Chem. Eng. J.*, 2016, **286**, 476–484.
58 Y. Chen, S.-R. Zhai, N. Liu, Y. Song, Q.-D. An and X.-W. Song, *Bioresour. Technol.*, 2013, **144**, 401–409.
59 E. Unur, *Microporous Mesoporous Mater.*, 2013, **168**, 92–101.
60 K. Foo and B. Hameed, *Chem. Eng. J.*, 2011, **166**, 792–795.
61 M. A. Islam, S. Sabar, A. Benhouria, W. Khanday, M. Asif and B. Hameed, *J. Taiwan Inst. Chem. Eng.*, 2017, **74**, 96–104.
62 A. Nasrullah, B. Saad, A. Bhat, A. S. Khan, M. Danish, M. H. Isa and A. Naeem, *J. Cleaner Prod.*, 2019, **211**, 1190–1200.
63 H. Deng, G. Li, H. Yang, J. Tang and J. Tang, *Chem. Eng. J.*, 2010, **163**, 373–381.
64 H. Li, L. Liu, J. Cui, J. Cui, F. Wang and F. Zhang, *RSC Adv.*, 2020, **10**, 14262–14273.
65 A. L. Cazetta, A. M. Vargas, E. M. Nogami, M. H. Kunita, M. R. Guilherme, A. C. Martins, T. L. Silva, J. C. Moraes and V. C. Almeida, *Chem. Eng. J.*, 2011, **174**, 117–125.
66 O. Üner, Ü. Geçgel and Y. Bayrak, *Water, Air, Soil Pollut.*, 2016, **227**, 1–15.
67 L. Liu, Y. Lin, Y. Liu, H. Zhu and Q. He, *J. Chem. Eng. Data*, 2013, **58**, 2248–2253.
68 E. N. El Qada, S. J. Allen and G. M. Walker, *Chem. Eng. J.*, 2008, **135**, 174–184.
69 E. N. El Qada, S. J. Allen and G. M. Walker, *Chem. Eng. J.*, 2006, **124**, 103–110.
70 S. Sahu, S. Pahi, S. Tripathy, S. K. Singh, A. Behera, U. K. Sahu and R. K. Patel, *J. Mol. Liq.*, 2020, **315**, 113743.